Phase resetting in a model of sinoatrial nodal membrane: ionic and topological aspects

MICHAEL R. GUEVARA AND HABO J. JONGSMA
Fysiologisch Laboratorium, Universiteit van Amsterdam, 1105 AZ Amsterdam, The Netherlands

GUEVARA, MICHAEL R., AND HABO J. JONGSMA. *Phase resetting in a model of sinoatrial nodal membrane: ionic and topological aspects.* Am. J. Physiol. 258 (Heart Circ. Physiol. 27): H734–H747, 1990.—We describe the phase-resetting effect of injecting an isolated current pulse in an ionic model of a single cell of the sinoatrial node. Delivery of a depolarizing pulse early (late) in the cycle results in a prolongation (abbreviation) of the cycle length. With a hyperpolarizing pulse, the effect is reversed. We determine the topological type or degree of phase resetting in two ways: *1*) by analyzing interbeat intervals extracted from the voltage waveform, and *2*) by analyzing the waveform, not only of the voltage, but of all the activation and inactivation variables. The two methods give similar results. At low (high) pulse amplitudes, there is type 1 (0) phase resetting. When type 1 phase resetting occurs, the new phase is a monotonically increasing function of the old phase at sufficiently low stimulus amplitudes, whereas at higher stimulus amplitudes it is not. Leading roles in generating phase resetting are attributed to the slow inward current and to the leakage current. Comparison is made with experimental phase-resetting findings in the sinoatrial node and other cardiac oscillators. Implications for unidirectional and bidirectional synchronization are also sketched out.

ionic mechanisms; graded action potentials; type 1 phase resetting; type 0 phase resetting; all-or-none depolarization; annihilation

---

OVER THE PAST SEVERAL DECADES, systematic phase-resetting experiments have been carried out on many biological oscillators (49). In a phase-resetting experiment, a stimulus of duration short in comparison with the characteristic period of the oscillator, is delivered to the oscillator. This perturbation results in a transient disturbance in the period of the oscillation, with recovery back to the original period eventually occurring. The stimulus, however, in general produces a permanent resetting of the timing or "phase" of the oscillator (readers unfamiliar with the concept of phase resetting should consult the APPENDIX for a brief introduction to the subject). Winfree (49) has shown that there are certain qualitative or topological features common to the phase-resetting data obtained from a wide variety of biological oscillators, from isolated pacemaker cells to circadian rhythms. These topological similarities exist even though the particular mechanisms operating in any two given oscillators might be completely different.

There have been several experimental studies on the phase-resetting response of the sinoatrial node (SAN) produced by stimulation with a current pulse (26, 35, 45, 47). There have also been a few reports in which this response has been modeled (5, 27, 36, 43). We investigate an ionic model that has not previously been studied (23), concentrating on the ionic mechanisms underlying phase resetting and on topological aspects of phase resetting. We have three main motivations for investigating the phase-resetting response of the model. The first is to lay the foundations for determining the extent to which topological characteristics of the response to an isolated current pulse (i.e., the phase-resetting response) can account for coupling patterns seen when a periodic train of current pulses is delivered. We have recently shown in experiments on embryonic chick heart cell aggregates that such topological considerations do indeed determine the various classes of patterns seen when periodic stimulation is imposed (13, 15, 17, 20, 21). For example, the type of phase resetting seen with a low-amplitude stimulus pulse accounts for the fact that Wenckebach-like rhythms are seen with low-amplitude periodic stimulation (20). At very high stimulus amplitudes, when there is a qualitative change in the topological characteristics of the phase-resetting response, one no longer sees Wenckebach rhythms but rather alternans rhythms (15, 21). At intermediate stimulus amplitudes, the topological characteristics are again different and account for the fact that chaotic rhythms and hysteresis can be seen (13, 15, 17, 21). It is thus of primary importance to characterize the topological features of phase resetting if one is to have any hope of making sense of the plethora of rhythms seen during periodic stimulation.

The second motivation for studying phase resetting is to use the phase-resetting response, once characterized, to investigate the extent to which the phasic influence of one spontaneously active SAN cell on another might be responsible for producing mutual synchronization in a population of two or more coupled nodal cells (15, 27, 36). A wide spectrum of coupling patterns can be seen in models of just two coupled oscillators (e.g., see Refs. 27, 36). The topological characteristics of phase resetting again play a major role in determining which classes of coupling patterns are seen at a given level of coupling (Guevara and Lewis, unpublished data).

Our third reason for studying phase resetting is that the study of phase resetting in an ionic model is interesting, indeed even valuable, in itself, because it can be used to determine the extent to which presently known ionic mechanisms, deduced from data obtained independently in voltage-clamp experiments, can account for experimentally observed behavior in phase-resetting ex-

periments. Discrepancies between theory and experiment might then point out new directions for modeling and perhaps even experimental work.

METHODS

We investigated the model of Irisawa and Noma (23), which is a modified version of the earlier model of Yanagihara, Noma, and Irisawa (51), incorporating especially a revised description of the slow inward current. We set the acetylcholine concentration to zero in the model. Numerical integration was carried out by implementing a variable time-step algorithm that is much more efficient than fixed time-step algorithms, producing equivalent accuracy with much less computation (48). In addition, the convergence of the algorithm for equations of the Hodgkin-Huxley type used in this model can be mathematically proven (48). By adjusting the integration time step (Δt) at any time t to be one of the nine values $2^N \cdot (0.032)$ ms with $0 \leq N \leq 8$, the change in the transmembrane potential (ΔV) in iterating from time t to time $t + \Delta t$ can be kept below 0.4 mV at the current pulse amplitudes employed in this paper. When ΔV is >0.4 mV, before the next iteration is carried out the time step is successively halved and the calculation redone until a value of ΔV <0.4 mV is achieved. When ΔV is <0.2 mV, the time step is doubled for the following iteration. In advancing from time t to time $t + \Delta t$, the current is calculated using the formula appearing in footnote 2 of Victorri et al. (48). The time step is adjusted to a nonstandard value [i.e., $\neq 2^N \cdot (0.032)$ ms] when a current pulse is injected so that the pulse is turned on and off at exactly the right times. L'Hôpital's rule is applied when necessary in calculating the rate constants α_m, α_f, β_p, α_q, and β_q as well as the leakage current I_l. Initial conditions are $V = -60.000$ mV, $m = 0.064260$, $h = 0.92720$, $d = 0.030477$, $f = 0.86991$, $p = 0.20890$, and $q = 0.012767$; the initial value of Δt is 4.096 ms. These initial conditions approximate, to five significant decimal places, a point on the limit cycle.

RESULTS

Figure 1 shows spontaneous activity in the model: the transmembrane potential (V), the total transmembrane current (I_{tot}), the fast inward sodium current (I_{Na}), the slow inward current (I_s), the potassium current (I_K), the hyperpolarization-activated current (I_h), and the time-independent background or leakage current (I_l). The interbeat interval is 329.2 ms; the maximum diastolic potential is −65.8 mV, and the overshoot potential is 18.3 mV. These values are close to those appearing in the original description of the model (23). When double-precision arithmetic is used instead of single precision (~15 vs. ~7 significant decimal digits), we obtain traces that superimpose with those shown in Fig. 1. In addition, decreasing the limits of the ranges of ΔV and Δt allowed by a factor of 10 using single-precision arithmetic, produces very little change in the waveform, with, for example, the spontaneous interbeat interval increasing by <1%. In what follows, we have therefore used single-precision computation and the ΔV range is 0.2 mV $\leq \Delta V \leq$ 0.4 mV.

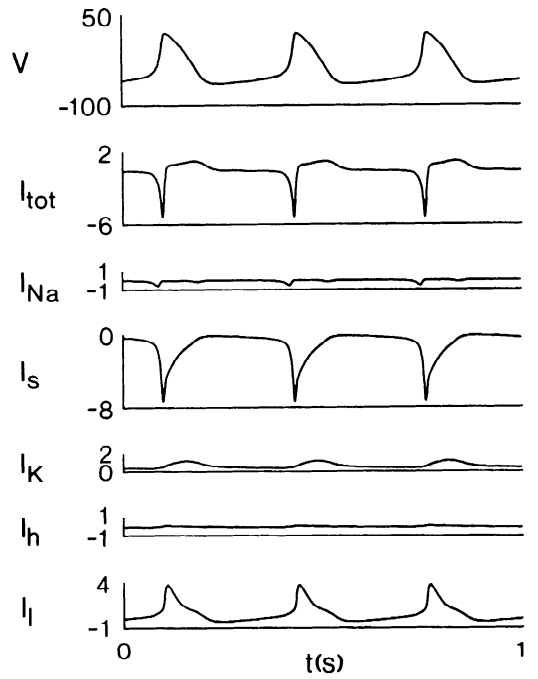

FIG. 1. Spontaneous activity in model. Transmembrane voltage (V) is in mV; all currents are in $\mu A/cm^2$ and are drawn to same scale. Inward currents are negative; outward currents are positive. Membrane capacitance is 1 $\mu F/cm^2$. I_{tot}, total transmembrane current; I_{Na}, fast inward sodium current; I_s, slow inward current; I_K, potassium current; I_h, hyperpolarization-activated current; and I_l, leakage current.

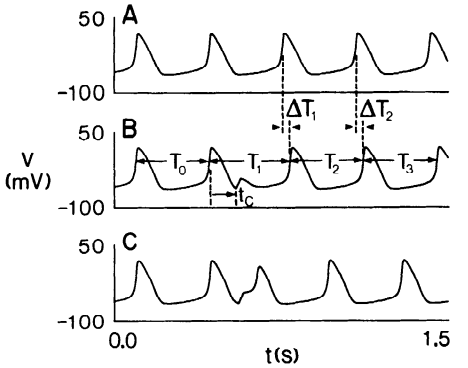

FIG. 2. Prolongation (B) and abbreviation (C) of cycle length produced by injecting a 20-ms-duration depolarizing current pulse of amplitude = −1.5 $\mu A/cm^2$. A: unperturbed activity. B: t_c = 120 ms, T_0 = 329.2 ms, T_1 = 364.8 ms, T_2 = 328.4 ms, and T_3 = 329.1 ms. C: t_c = 130 ms, T_0 = 329.2 ms, T_1 = 213.0 ms, T_2 = 329.7 ms, and T_3 = 329.2 ms. V, transmembrane voltage.

Note that during diastolic depolarization the changes in I_s and I_l are of comparable magnitude but are oppositely directed. The changes in I_K, I_{Na}, and I_h are much smaller, with I_K changing considerably more than either I_{Na} or I_h. In fact, I_{Na} and I_h contribute little to the overall activity; removing them both from the model causes small changes in the waveform of the action potential and increases the spontaneous interbeat interval by ~20%.

Figure 2 shows that injection of a 20-ms-duration depolarizing current pulse can lengthen (B) or shorten (C) the interbeat interval, depending on the phase in the cycle at which it is injected. We define the interbeat interval to be the time between successive crossings of −10 mV on the upstroke phase of the action potential

(the "event marker"). The spontaneous interbeat interval is denoted by T_0, the perturbed interbeat interval by T_1, and the first poststimulus interbeat interval by T_2 (Fig. 2). The coupling interval is the time from the crossing of −10 mV on the upstroke of the action potential immediately preceding the stimulus to the beginning of the stimulus itself and is denoted by t_c. The normalized coupling interval t_c/T_0 is called the old phase, and is denoted by Φ, which has the range $0 \leq \Phi < 1$. All intervals are given in milliseconds. The amplitude of the current pulse in microamperes per centimeter squared is denoted by A, with a negative amplitude corresponding to a depolarizing stimulus. Stimulus amplitude increases when the absolute value of A increases.

The temporal shifts ΔT_1 and ΔT_2 are defined as indicated in Fig. 2. Thus

$$\Delta T_1 = T_0 - T_1 \quad (1)$$

and

$$\Delta T_2 = (T_0 - T_1) + (T_0 - T_2) \quad (2)$$

More generally

$$\Delta T_i = \sum_{j=1}^{i} (T_0 - T_j) \quad (3)$$

Note that in Fig. 2, $T_2 \simeq T_0$, and so $\Delta T_2 \simeq \Delta T_1$. Also note that ΔT_1 is negative for $T_1 > T_0$ ("delay") and positive for $T_1 < T_0$ ("advance"). Each column of Fig. 3 shows the effect of systematically increasing t_c from 60 to 180 ms in steps of 20 ms at a fixed amplitude of the current pulse (a "phase-resetting run"). Phase-resetting runs at three different amplitudes (−1.0, −1.5, and −2.0 μA/cm^2) are shown. At all three amplitudes, for $t_c < 60$ ms (not shown), T_1 is slightly larger than T_0, whereas for $t_c > 180$ ms (not shown), the pulse is suprathreshold, and so $T_1 \simeq t_c$.

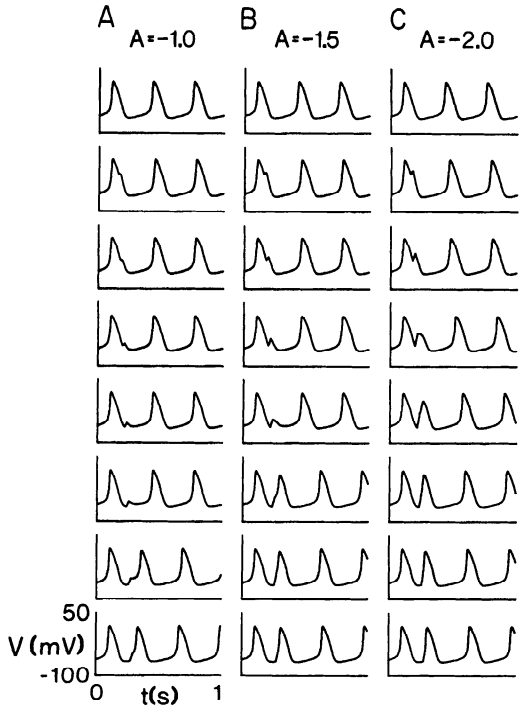

FIG. 3. Phase-resetting runs at 3 different current amplitudes (A) with t_c incremented in steps of 20 ms from 60 ms (2nd row) to 180 ms (bottom row). Top row shows unperturbed activity. A: A = −1.0 μA/cm^2; B: A = −1.5 μA/cm^2; and C: A = −2.0 μA/cm^2.

We have investigated in some detail the way in which prolongation of cycle length turns into abbreviation as t_c is increased at each of the three amplitudes shown in Fig. 3. At the two lower amplitudes, one sees a gradual smooth transition from maximal prolongation to maximal abbreviation of cycle length. However, as stimulus amplitude increases, one needs an increasingly smaller increment in t_c to demonstrate this continuity. For example, at $A = -1.0$ μA/cm^2 (Fig. 4B), an increment in t_c of ~2.0 ms is sufficient to reveal the continuity, but at $A = -1.5$ μA/cm^2 (Fig. 4C) one must employ an increment in t_c of 0.1 ms.

At the highest amplitude used in Fig. 3 ($A = -2.0$ μA/cm^2) the current pulse is suprathreshold throughout diastole. Maximal prolongation of cycle length does not then occur via a prolongation of the duration of diastole as at the two lower stimulus amplitudes (Fig. 4); instead, it occurs via a prolongation of action potential duration. Figure 5 shows voltage tracings at values of t_c in the neighborhood of the transition from maximal prolongation to maximal abbreviation of interbeat interval at $A = -2.0$ μA/cm^2. These tracings highlight methodological problems in determining the interbeat interval. It can be seen that the voltage tracing is changing in a nicely continuous manner in Fig. 5, with the amplitude of the graded waveform smoothly increasing as t_c increases. Yet, there is arbitrariness involved in deciding at what coupling interval the event provoked by the stimulus is to be called an action potential. One criterion might be to say that an action potential occurs when there is some "active" response, i.e., when the membrane continues to depolarize after the termination of the current pulse. In that case, the transition from prolongation to abbreviation of cycle length at $A = -2.0$ μA/cm^2 would occur somewhere between $t_c = 100$ ms and $t_c = 102$ ms in Fig. 5. By our criterion of a positive-going crossing of −10 mV, the transition occurs somewhere between 104 and 110 ms.

We now investigate topological aspects of the phase-resetting response of the model (see APPENDIX as well as

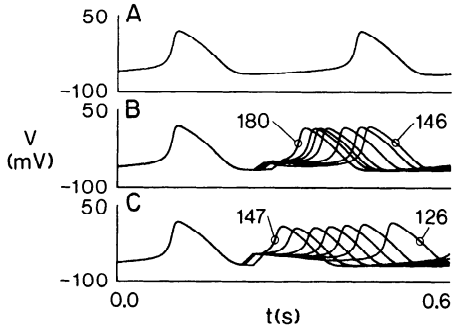

FIG. 4. Parts of phase-resetting runs shown in Fig. 3, A and B, but with finer increments in t_c. A: unperturbed activity; B: amplitude = −1.0 μA/cm^2, with t_c = 146, 154, 156, 158, 162, and 180 ms; and C: amplitude = −1.5 μA/cm^2, with t_c = 126, 126.2, 126.3, 126.5, 127, 130, and 147 ms. Smallest and largest values of t_c used in B and C result in maximal prolongation and abbreviation of cycle length, respectively, at these 2 amplitudes.

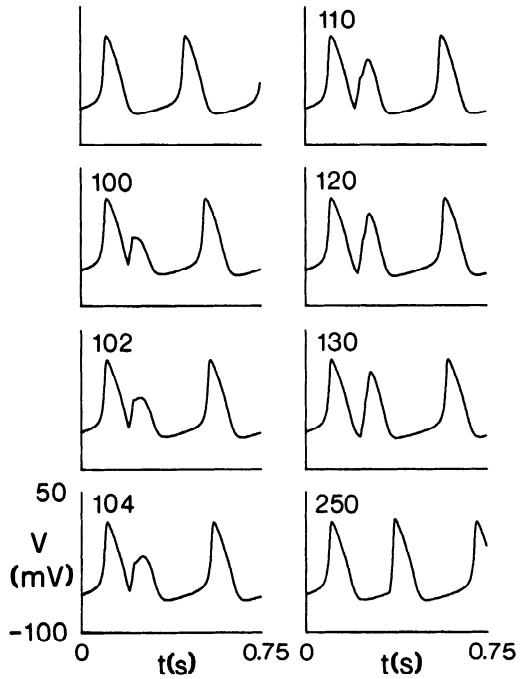

FIG. 5. Part of phase-resetting run shown in Fig. 3*C* (amplitude = -2.0 μA/cm^2), but with t_c changed more finely. Top left-hand trace shows unperturbed activity; value of t_c in ms is indicated on other traces.

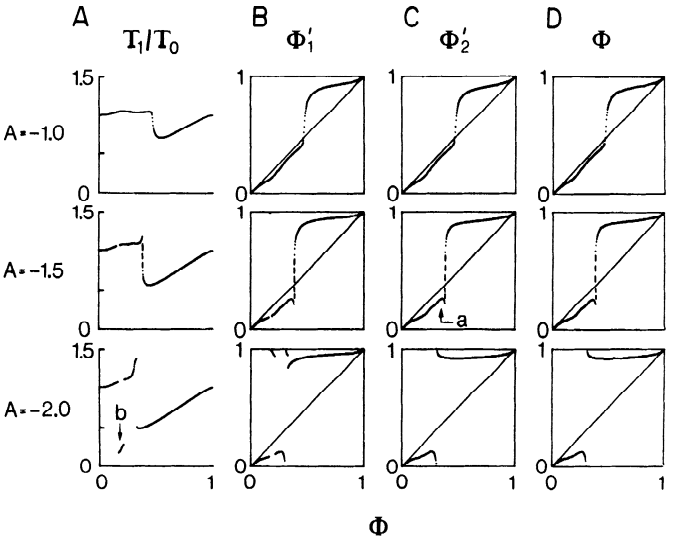

FIG. 6. Plots of normalized perturbed interbeat interval T_1/T_0 (*A*), 1st transient phase Φ'_1 (*B*), 2nd transient phase Φ'_2 (*C*), and directly computed new phase Φ' (*D*) at 3 different stimulus amplitudes: A = -1.0 (top row), -1.5 (middle row), and -2.0 (bottom row) μA/cm^2. Coupling interval is incremented in steps of 1 ms; Φ denotes the old phase t_c/T_0. Labeled arrows indicate features described in text. Dashed lines in middle row indicate where data points fall when t_c is changed in steps of 0.1 ms. In *D*, data points were calculated from initial conditions $V = -10.000$ mV, $m = 0.92806$, $h = 0.0017017$, $d = 0.67194$, $f = 0.76323$, $p = 0.17147$, $q = 0.015129$, and $\Delta t = 0.064$ ms, as described in text.

Refs. 14, 15, 18, 31, 49, 50 for background material). The first transient phase Φ'_1 is defined by

$$\Phi'_1 = \Phi + \Delta T_1/T_0 \quad \text{(modulo 1)} \qquad (4)$$

the second transient phase Φ'_1 by

$$\Phi'_2 = \Phi + \Delta T_2/T_0 \quad \text{(modulo 1)} \qquad (5)$$

and the ith transient phase Φ'_i by

$$\Phi'_i = \Phi + \Delta T_i/T_0 \quad \text{(modulo 1)} \qquad (6)$$

where ΔT_1, ΔT_2, and ΔT_i are as defined in Fig. 2 and *Eqs. 1–3*. We define the modulo 1 operation to be such that x (modulo 1) is given by $x - [x]$, where $[x]$ is the integer, positive or negative, produced by truncating x (i.e., discarding its fractional part). With this definition of the modulo 1 operation, the result given by *Eqs. 4–6* can be negative; one must therefore add 1 to the result in that case, to ensure that Φ'_i lies in the range $0 \leq \Phi'_i < 1$ (see APPENDIX). Figure 6 shows the normalized perturbed interbeat interval T_1/T_0 (first column), Φ'_1 (second column), and Φ'_2 (third column) at the three amplitudes of stimulation previously considered when t_c is changed with an increment of 1 ms. A curve drawn through the $\Phi'_1(\Phi'_2,\Phi'_i)$ is referred to as the first (second, ith) transient phase transition curve, abbreviated PTC_1 (PTC_2, PTC_i).

Note that there are artifacts present in the first and second columns of Fig. 6 at $A = -1.5$ and -2.0 μA/cm^2. For example, at $A = -2.0$ μA/cm^2, there is artifactual shortening of the normalized perturbed interbeat interval T_1/T_0 for Φ in the range of $0.17 < \Phi < 0.21$ (segment of data indicated by arrow labeled b). This is because the voltage crosses -10 mV during the current pulse (e.g., Fig. 3*C*; $t_c = 60$ ms), and so an event occurs, resulting in a value of T_1 only slightly larger than t_c. However, this cannot be said to be a real shortening of the cycle length, because the membrane resumes its repolarizing time course immediately on termination of the current pulse. In the reverse manner, at $t_c = 104$ ms (Fig. 5), the voltage does not cross -10 mV; thus a prolongation of cycle length, which might be said to be artifactual, results. The artifactual shortenings produce jump discontinuities of <1 cycle length in the curves of T_1/T_0 and Φ'_1 in Fig. 6 at $A = -1.5$ and -2.0 μA/cm^2 (e.g., at both ends of the segment labeled b in the left column at $A = -2.0$ μA/cm^2 and of the analogous segment at $A = -1.5$ μA/cm^2). A second kind of discontinuous jump, also of <1 cycle length, occurs in the plot of T_1/T_0 at -2.0 μA/cm^2 at $\Phi \simeq 0.33$, where maximal prolongation of cycle length discontinuously turns into shortening of cycle length as Φ is increased (Fig. 5). An apparently similar jump appears in the plot of T_1/T_0 at $A = -1.5$ μA/cm^2. This jump however is not real, because in this case there are actually data points lying in the apparent gap in the curve of data points. These points lie along the dashed line indicated in Fig. 6 (middle row) and can be seen only if t_c is changed in steps of a fraction of a millisecond (Fig. 4*C*).

The first kind of discontinuity [e.g., seen at the edges of the segment labeled b in Fig. 6 (bottom row)] is a compulsory feature of phase-resetting data (15, 18, 19, 31) and is a consequence of the fact that some precise but arbitrary definition of an event marker must be taken. However, this form of discontinuity in T_1/T_0 and in PTC_i is expected to disappear in the limit $i \rightarrow \infty$ (see APPENDIX). In fact, no such discontinuities are apparent on PTC_2 (Fig. 6*C*), indicating that the trajectory returns to the immediate vicinity of the limit cycle very quickly

in this model after a perturbation. In addition, on the scale of Fig. 6, the calculated values of Φ'_3 (not shown) superimpose with those of Φ'_2. One can thus take PTC_2 as a very good approximation to PTC_∞, the "new phase-old phase" curve (see APPENDIX), with Φ'_∞ being termed the new or eventual phase (49).

Note that the transient phases Φ'_i are calculated using *Eqs. 4–6* by inspecting only the voltage waveform; no account is taken of the activation variables *m, d, p,* and *q* and the inactivation variables *h* and *f*. Because these other variables are not measurable during phase-resetting experiments, these formulas involving only *V* must of necessity be used in experimental work. However, in modeling work we can make use of the additional information contained in these other variables, which are then accessible, to more directly and perhaps more accurately compute the new phase.

We now outline this method, which has previously been used in studying neural (2, 16) and simple two-dimensional (16) limit-cycle oscillators. First, starting at $t = 0$ from initial conditions appropriate to the point $V = -10$ mV on the upstroke of the action potential, the equations of the model are numerically integrated for one full cycle of spontaneous activity. At each iteration, the values of the time *t* and of the variables *V, m, h, d, f, p,* and *q* at that time are stored in an array. There are 623 points on the limit cycle stored in this way. Second, integration is restarted from the same initial conditions, and a current pulse is injected at a coupling interval t_c. The integration is then carried forward for a total time $t_c + T_0$ (with $T_0 = 329.2$ ms as before), and the coordinates (*V, m, h, d, f, p,* and *q*) of the state point of the system at the end of this second integration are stored. A search is then made through the array of 623 points stored initially to find the one that is nearest to this terminal point. We use as our measure of the distance between two seven-dimensional points $X_1 = (V_1, m_1, h_1, d_1, f_1, p_1,$ and $q_1)$ and $X_2 = (V_2, m_2, h_2, d_2, f_2, p_2,$ and $q_2)$ the usual Euclidean metric

$$|X_1 - X_2| = \{[0.01(V_1 - V_2)]^2 + [m_1 - m_2]^2 + [h_1 - h_2]^2 + [d_1 - d_2]^2 + [f_1 - f_2]^2 + [p_1 - p_2]^2 + [q_1 - q_2]^2\}^{1/2} \quad (7)$$

The weighing factor of 0.01 is included because the range of the voltage variable is about two orders of magnitude larger than that of the other variables, which have a range from zero to one. Once the closest point on the limit cycle is thus found, we assign the phase of that point, which is simply t_c/T_0 from the first integration carried out, to be the new phase Φ' corresponding to the old phase $\Phi = t_c/T_0$. This second integration and subsequent search is then repeated for a new value of t_c.

Figure 6*D* shows the new phase calculated in this direct way at three different amplitudes of stimulation with t_c changing in steps of 1 ms. Data points superimposable with these are found if, in the second integration step described above, the integration is carried forward for a time $t_c + 2T_0$ instead of $t_c + T_0$. This once again indicates that the limit cycle is strongly attracting, and that the points in Fig. 6*D* are indeed a very good approximation to the new phase. Note that there are negligible differences between the new phase found in the direct way (*D*) and that computed from the voltage waveform alone (*C*) using *Eq. 5*. This indicates that the voltage waveform alone can be safely used to calculate the new phase: access to the other variables is not absolutely crucial. Note however that Φ'_2, and not Φ'_1, must be used to obtain a good approximation to the new phase when the voltage waveform alone is analyzed. Note also that, when the direct method is used, artifactual discontinuities of the sort resulting when the method involving analysis of interevent intervals is used (Fig. 6*B*) do not occur.

At the lower two amplitudes of Fig. 6 (first and second rows), type 1 phase resetting occurs, because the average slope of PTC_2, which is a good approximation to PTC_∞, is unity (see APPENDIX). Note that the simulations shown in Fig. 4*C* imply that data points would fall along the dashed line appearing at $\Phi \simeq 0.4$ in all panels of the second row of Fig. 6 where t_c is changed with increments smaller than 1 ms. At the lowest amplitude ($A = -1.0$ $\mu A/cm^2$), Φ'_2 increases monotonically, whereas at the intermediate amplitude ($A = -1.5$ $\mu A/cm^2$), it does not: a downturning in the curve appears at $\Phi \simeq 0.35$ (arrow labeled a). At $A = -2.0$ $\mu A/cm^2$ (third row), the average slope of PTC_2 is zero, and type 0 phase resetting is said to occur (see APPENDIX). The transition from type 1 to type 0 phase resetting occurs at an amplitude just below $A = -1.8$ $\mu A/cm^2$. At $A = -1.8$ $\mu A/cm^2$, incrementing small-amplitude oscillatory activity can be seen immediately after delivery of the current pulse (Fig. 7*B*), which is consistent with the fact that one is close to the type 1/type 0 border at this amplitude (see APPENDIX).

We now turn to investigation of the ionic mechanisms underlying phase resetting. Figure 8 shows the ionic basis of the lengthening (*A*) and shortening (*B*) of cycle length produced by injecting a current pulse of intermediate amplitude ($A = -1.5$ $\mu A/cm^2$) during diastolic depolarization. At $t_c = 120$ ms (*A*), the total current lies just outward at the end of the current pulse, producing a negative rate of change in transmembrane potential (dV/dt) and a prolongation of cycle length. In contrast, at $t_c = 130$ ms (*B*), the total current lies just inward, producing a positive dV/dt that leads to premature activation of I_s and a shortening of the interbeat interval. In both instances, injection of the current pulse produces almost

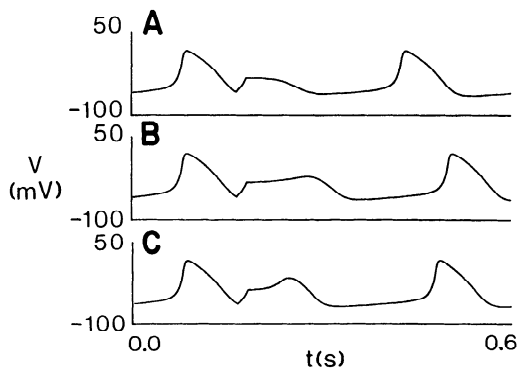

FIG. 7. Waveforms near type 1/type 0 border. Amplitude = -1.8 $\mu A/cm^2$ and $t_c = 108$ ms (*A*), 109 ms (*B*), and 110 ms (*C*). *V*, transmembrane voltage.

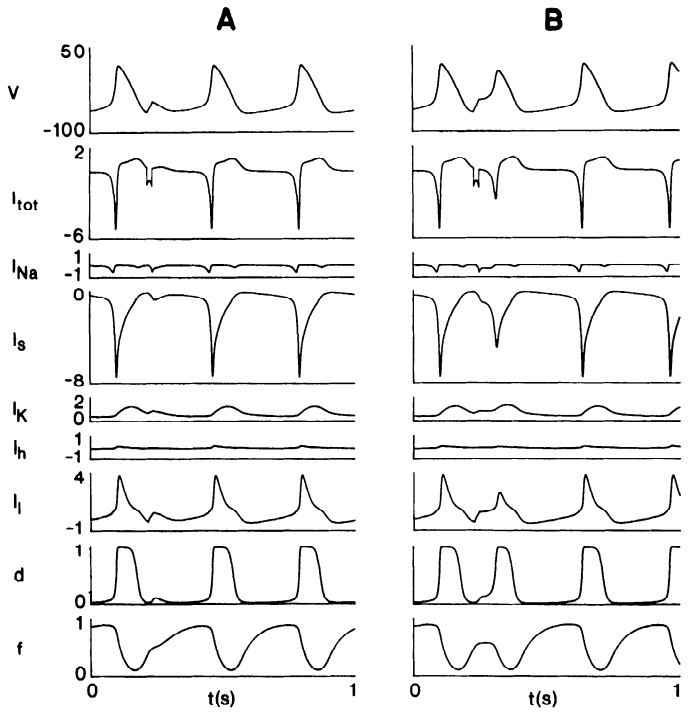

FIG. 8. Ionic basis of transition from prolongation to abbreviation of cycle length. Voltage V is in mV. All currents are in $\mu A/cm^2$ and drawn to same scale. Activation and inactivation variables d and f of slow inward current (I_s) are shown. A stimulus pulse with amplitude = -1.5 $\mu A/cm^2$ is injected at t_c = 120 ms (A) and at t_c = 130 ms (B).

equal, but oppositely directed, changes in I_s and I_l. The increase in I_l is simply caused by the fact that I_l is outward and has a positive-slope current-voltage (I-V) relationship. The increase in the magnitude of I_s is caused by two factors. *1*) I_s is inward and its I-V curve has a negative slope over this range of potentials (see Fig. 6*B* of Ref. 23). *2*) There is increased activation (i.e., increase in the activation variable d) and decreased inactivation (i.e., increase in the inactivation variable f) of I_s during the current pulse (Fig. 8). In addition, the potential at the end of the current pulse is ~−44 mV at t_c = 120 ms and −43 mV at t_c = 130 ms, which is about where the foot of the activation curve for I_s is situated (see Fig. 1 of Ref. 23). Thus the fine balance between the changes in I_s and I_l produced during the current pulse together with the setting of the voltage by the current pulse into the region of activation of the large current I_s makes it possible for small changes in t_c to result in significant changes in the perturbed interbeat interval T_1 at this current amplitude (Fig. 4*C*).

Note that during injection of the current pulse, the changes in I_{Na}, I_K, and I_h are smaller than those in I_s and I_l; moreover, these changes are not appreciably different when either prolongation or abbreviation of cycle length is produced. In fact, if I_{Na} and I_h are removed from the model, traces of V, I_{tot}, I_s, I_K, and I_l very similar to those shown in Fig. 8 still result. This indicates that in this model the major ionic mechanisms underlying prolongation and abbreviation of interbeat interval (as well as the rapid transition from the former to the latter) involve I_s, I_l, and, to a lesser extent, I_K.

The decrease in the amplitude and the overshoot potential of the graded action potential of Fig. 8*B* is largely caused by the decrease in the magnitude of I_s. This decrease is in turn caused by the markedly decreased rate of removal of inactivation (in fact, the inactivation variable f is almost constant in time) produced immediately after injection of the current pulse (see bottom trace of Fig. 8*B*). Once again I_l is playing a compensatory role with respect to I_s, with, for example, its peak value being less outward than during unperturbed activity. As t_c is increased beyond 130 ms, the overshoot potential and the maximal rate of rise of the upstroke phase of the action potential ($\dot{V}_{max}$) both gradually increase (see Fig. 3*B*; t_c = 140, 160, and 180 ms). This is primarily caused by a progressive recovery of the I_s waveform back to its normal shape. Indeed, for t_c greater than ~230 ms, the overshoot potential and the peak value of the total current (and hence $\dot{V}_{max}$) actually increase beyond their normal values. This also occurs at higher current amplitudes where the pulse is suprathreshold throughout diastole (e.g., Fig. 5; t_c = 250 ms). These increases are caused by a direct effect of the current pulse and an increase in I_{Na}; I_s remains slightly depressed even for t_c very close to T_0.

The maximum diastolic potential (MDP) of a graded action potential elicited early in diastole (e.g., Fig. 5; t_c = 120 ms) is slightly more negative (by ~1 mV) than that of an action potential during unperturbed activity and is followed by a diastolic duration (i.e., time from MDP to subsequent upstroke) of the poststimulus cycle that is slightly longer than usual. Despite this prolongation of the diastolic interval, the poststimulus interbeat interval T_2 is still reduced below T_0 because the action potential duration is reduced much more than the diastolic duration is increased (e.g., T_2 = 316 ms at t_c = 120 ms in Fig. 5).

We have also investigated the ionic basis of the prolongation of cycle length produced when a large amplitude pulse is delivered during the action potential (e.g., Fig. 3*C*; t_c = 80 ms). This prolongation is largely caused by an increase in the action potential duration; the diastolic time of the perturbed cycle is only slightly increased. As is the case when a very premature graded action potential is elicited, this increase in the diastolic time is associated with a slight increase in the negativity of the MDP. The effect of the current pulse is basically to reset the various activation and inactivation variables backwards in time; when the injection of current ends, the membrane then resumes repolarizing at more or less the usual rate appropriate to the voltage at that time. During the current pulse, there is an increase in I_s that is almost exactly balanced by an increase in the sum of I_K and I_l.

Even though we have concentrated above on the response of the model to a depolarizing stimulus, we have also investigated, in lesser detail, the response to a hyperpolarizing stimulus. The motivation for doing so comes from the fact that nodal cells are normally subject to vagal stimulation, which is hyperpolarizing. Also, during spontaneous activity, at any one time some cells of the node will be more depolarized than others; this former group of cells will be subject to the hyperpolarizing influence of the latter (see Fig. 2-21 of Ref. 15).

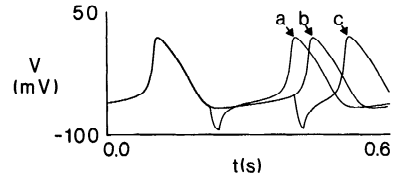

FIG. 9. Phase-resetting effect of injecting a hyperpolarizing current pulse. Either shortening (*trace a*, t_c = 120 ms) or prolongation (*trace c*, t_c = 300 ms) of cycle length can be seen, depending on coupling interval. amplitude = 4.0 $\mu A/cm^2$. *Trace b* shows unperturbed activity.

Figure 9 shows that the response to injection of a hyperpolarizing pulse is the opposite to that of a depolarizing pulse, in that a stimulus falling early (*trace a*) in the cycle produces a shortening of cycle length, whereas one falling later (*trace c*) produces a prolongation. The transition from type 1 to type 0 phase resetting occurs at a higher stimulus amplitude than with a depolarizing stimulus.

CONCLUSIONS

Comparison with experimental results. The computations presented above demonstrate that the phase-resetting response of the model of Irisawa and Noma has much in common with that experimentally observed in the SAN. We now summarize what we see to be the five main correspondences, mentioning one discrepancy.

1) The response is biphasic, with a depolarizing current pulse producing a lengthening of cycle length if applied early in the cycle and a shortening if applied later (model, Figs. 2–8; see also Refs. 27, 36, 43 for similar results in other SAN models; experiment, Refs. 26, 45, 47). A similar biphasic effect of ventricular systole on the SAN cycle during complete heart block has also been documented in human beings (data of Roth and Kisch, 1948, plotted in Fig. 11-32*A* of Ref. 1; Ref. 22) and has been attributed, among other things, to the action of ventricular currents on the SAN (22). The phase in the P-P cycle at which the QRS complex must fall to produce a prolongation or an abbreviation of the P-P interval is consistent with that interpretation.

In contrast, in both experimental and modeling work on Purkinje fiber, the phase-resetting response is usually triphasic, because a slight shortening of action potential duration, and hence of cycle length, is seen when a relatively large amplitude depolarizing stimulus falls very early in the cycle (18). It is thus perhaps not coincidence that a similar triphasic response is also found in a model of the SAN derived by modifying a model of Purkinje fiber (Fig. 9*A* of Ref. 5). In addition, a quinquephasic response can be seen in Purkinje fiber when supernormal excitability occurs (18). We know of no experimental evidence for either triphasic or quinquephasic responses in the SAN. The biphasic response of the SAN is reversed when a hyperpolarizing current pulse is applied, in that a stimulus falling relatively early in the cycle produces an advance, whereas the same stimulus delivered later in the cycle results in a delay (model, Fig. 9; see also Refs. 5, 36, 43; experiment, Ref. 26). Whereas delays have often been seen with vagal stimulation, which is hyperpolarizing in nature, advances have been reported only infrequently.

The maximal prolongation that we have seen in the model when changing the pulse amplitude in steps of 0.1 $\mu A/cm^2$ and t_c in steps of 1 ms occurs at t_c = 109 ms and $A = -1.8$ $\mu A/cm^2$, producing T_1/T_0 = 1.89 (Fig. 7*B*). Whereas prolongations of as much as 80% (i.e., T_1/T_0 = 1.8) have been reported in experimental work on the SAN (26), the corresponding voltage tracings were not shown, and thus we cannot say whether small-amplitude oscillatory activity of the type shown in Fig. 7*B* is associated experimentally with such long prolongations. This oscillatory activity is not unexpected near the type 1/type 0 border and is presumably caused by the proximity of the trajectory, at the time the current pulse is turned off, to the stable manifold of the equilibrium point lying at $V \simeq -34$ mV (see APPENDIX). Similar behavior has been previously described in ionic models of the SAN (5, 43) and Purkinje fiber (18) and in experimental and modeling work on embryonic chick ventricular heart cell aggregates (10, 15, 19). However, in the latter case, the oscillatory activity is in the pacemaker rather than the plateau range of potentials, as is an equilibrium point.

2) As the amplitude of a depolarizing stimulus is increased, the phase in the cycle at which lengthening of cycle length turns into shortening decreases, and the range of Φ over which this transition occurs also decreases (model, Figs. 3, 4, and 6; see also Refs. 5, 36, 43; experiment, Refs. 26, 45). Similar behavior has been reported in Purkinje fiber (28), in ventricular heart cell aggregates (19), and in models thereof (10, 15, 18). In fact, in those cases the response can become so abrupt as to be effectively discontinuous; for example, in a model of the aggregate, intermediate responses spanning the diastolic interval (analogous to those shown in Fig. 4*C*) are not seen in a certain range of amplitudes when t_c is changed with an increment as small as 1 μs (Fig. 3-9 of Ref. 15). Such abrupt behavior is not seen in the SAN model; this difference is probably connected with the fact that I_{Na} has been implicated in generating such behavior (10), and I_{Na} in the SAN model is much smaller than in models of tissue of ventricular origin.

3) Graded action potentials are seen in response to high amplitude depolarizing stimulation (model, Figs. 3 and 5, see also Ref. 5; experiment, Refs. 4, 11, 26, 32, 35, 47). The overshoot potential and $\dot{V}_{max}$ tend to increase as t_c is increased; in fact, they exceed the control value if t_c is made sufficiently large (model, Fig. 5; experiment, Refs. 11, 35). Graded action potentials can also be seen in response to a hyperpolarizing stimulus when an anodal-break effect is produced. As the amplitude of the hyperpolarizing pulse is increased at fixed t_c, there can be a progressive fall in the overshoot of the action potential (model, not shown; experiment, Fig. 3*A* of Ref. 26). A rise in the overshoot can also be seen in the model (not shown) for other combinations of stimulus amplitude and timing (see also Fig. 6*B* of Ref. 5).

4) Annihilation of activity with a single current pulse is not possible in the model studied above, because clamping the membrane to the zero-current potential, setting all activation and inactivation variables to the asymptotic values appropriate to that potential, and then releasing the clamp results in the resumption of sponta-

neous activity. This result also occurs in the precursor to the model studied here (Fig. 9 of Ref. 51) and is in agreement with the corresponding experimental finding (39). Note that the model studied here is formulated using voltage-clamp data from the same experimental preparations in which this behavior was found experimentally. There is one report of annihilation in strips of tissue taken from the kitten SAN (24); the model considered in this paper (23) can be made to show annihilation if it is suitably modified (unpublished data).

5) In the model, the stimulus pulse has only a slight effect on the poststimulus and subsequent cycles at lower stimulus amplitudes, i.e., $T_i \simeq T_0$ for $i \geq 2$. This is reflected in Fig. 6*B* ($A = -1.5$ μA/cm^2), where Φ'_1 and Φ'_2 are nearly identical, indicating $T_2 \simeq T_0$. At higher stimulus amplitudes (e.g., $A = -2.0$ μA/cm^2), T_2 can be considerably less than T_0 when a graded action potential is produced (cf. Φ'_1 and Φ'_2 in bottom row of Fig. 6). This is caused by the large decrease in action potential duration, which overrides the slight increase of diastolic duration of the poststimulus cycle (Fig. 5). This increase in diastolic duration is associated in the model with a slightly more negative MDP of the graded action potential. Whereas concurrent increases in the negativity of MDP and the diastolic duration have been reported (e.g., Fig. 7*D* of Ref. 26), prolongation of diastolic duration is more often associated with an MDP depolarized beyond its usual value (e.g., Refs. 4, 11, 33). In these cases, the diastolic duration can be prolonged to the extent that significant "depression of automaticity" (42) of the SAN occurs. We have not seen such effects in our modeling work.

Ionic mechanisms underlying phase resetting. The ionic mechanisms underlying phase resetting in the model studied here are similar in some instances to those responsible for analogous behaviors in models of other cardiac oscillators. For example, the mechanisms responsible for the prolongation of action potential duration (e.g., Fig. 3*C*; $t_c = 80$ ms) and for the production of graded action potentials (Figs. 3, 5, and 8) are similar to those operating in a model of Purkinje fiber (18). In contrast, the mechanisms operative in the pacemaker range of potentials (illustrated in Fig. 8) are quite different from those operating in models of Purkinje fiber (18) and heart cell aggregates (10) when similar voltage traces are seen; in both those instances the pacemaker current I_h (or I_f or I_{K_2}) is a major factor. However, a feature common to both these classes of models is that the current pulse produces almost equal, but oppositely directed, changes in the two major currents involved in generating diastolic depolarization (I_s and I_1 in the SAN model, I_{K_2} and I_1 in the Purkinje fiber and aggregate models).

At this point, we must stress that the SAN is an inhomogeneous structure, both histologically and electrophysiologically (3). For example, action potentials of different morphologies are found in different parts of the node during spontaneous activity. Recording from small pieces cut from the node reveals that these differences are to a large extent intrinsic, because the morphology of the action potentials recorded from any piece are quite similar to those recorded in situ at the parent location in the intact node (34). In addition, the response to electrical stimulation of small pieces coming from different parts of the node can be quite different (34, 35). The model investigated above was based on data obtained from voltage-clamp work on small pieces probably taken in large part from regions of the node displaying latent pacemaker activity, because pieces dissected from the dominant pacemaker region apparently only rarely recover their spontaneous activity (35). Thus the model of Irisawa and Noma (23), or for that matter any other model of SAN cells, should not be regarded as representative of the SAN as a whole, because of the above mentioned inhomogeneities. In particular, in cells of the SAN (6, 35) and models thereof (38, 43) in which I_h is more implicated in generating diastolic depolarization, one would expect to have a mechanism of phase resetting involving I_h when a subthreshold current pulse is delivered during diastole similar to that previously described in heart cell aggregates (10). One recent modeling study on the SAN has indeed claimed that effects caused by I_h are important in phase resetting (43). In addition, in the more peripheral regions of the node, where I_{Na} is present to a greater degree, one might expect to see an abrupt transition from prolongation to abbreviation of cycle length when a current pulse of intermediate amplitude is delivered, similar to that recently described in heart cell aggregates (15, 19) and Purkinje fiber (18). Indeed, in a study on the precursor (51) of the model studied here, a more significant role was attributed to I_{Na} when behavior similar to that shown in Fig. 8 was analyzed (36).

The model studied here (23) does not contain currents included in other models, e.g., the Na^+-K^+ pump current (38), the Na^+-Ca^{2+} exchange current (38), and the transient-type calcium current (37), which can have an effect on the beat rate; nor are the various ionic concentrations allowed to fluctuate as in one other model (38). Although preliminary calculations performed by us on both of these models (37, 38) show no major changes in the phase-resetting characteristics, we cannot rule out at this time the possibility that there might be one or more aspects of phase resetting that would be influenced by these modifications.

The topology of phase resetting. In many experimental and modeling studies, plots of T_1/T_0 similar to that shown in Fig. 6 (top row) have been found; these findings are consistent with the existence of type 1 phase resetting. In fact, for any limit-cycle oscillator, type 1 phase resetting is obligatory at a sufficiently low stimulus amplitude (see APPENDIX). Patterns of activity very similar to that shown in Fig. 3*C* have also been seen many times in the SAN (e.g., Refs. 4, 11, 32, 33). We have identified such behavior, in which graded action potentials are produced by stimuli falling relatively early in the cycle, as corresponding to type 0 phase resetting (Fig. 6, bottom row). Similar voltage waveforms showing graded action potentials are also seen during type 0 phase resetting in reaggregates of trypsin-dispersed embryonic chick ventricular cells (15, 19) and in both experimental and modeling work on Purkinje fiber (18).

The direct calculation of the new phase-old phase

curve (Fig. 6*D*) has not previously been carried out for a cardiac oscillator. Such a calculation cannot be carried out in experimental work. Fortunately, the calculations show that consideration of the voltage waveform alone, which is experimentally measurable, gives results very similar to the full-blown seven-dimensional calculation (cf. data in *C* and *D* of Fig. 6). This finding is probably connected in some way with the fact that the voltage variable plays a role disproportionate to that of any other variable in models of the Hodgkin-Huxley type.

Our modeling work indicates that determination of T_1 alone, which is the common practice, is not sufficient to ascertain the type of phase resetting present near the border between type 1 and type 0 phase resetting; for example, the T_1/T_0 data at $A = -1.5$ $\mu A/cm^2$ and $A = -2.0$ $\mu A/cm^2$ in Fig. 6*A* look quite similar, but in the former case type 1 phase resetting occurs, whereas in the latter case there is type 0 phase resetting. In addition, at these two stimulus amplitudes, changing t_c in steps as small as 1 ms is not sufficient to determine the type of phase resetting present; increments of less than 1 ms are required (e.g., Fig. 4*C*). In all previous experimental and modeling work on the SAN, t_c was not changed sufficiently finely in the transitional range of coupling intervals (as in Fig. 4) to determine the type of phase resetting present. This suggests that previous identifications (24, 43, 50) of phase-resetting behavior as being of type 0 in the SAN were premature.

The transition from type 1 to type 0 phase resetting reported above is direct, in that it takes place at a single well-defined value of the stimulus amplitude (just below $A = -1.8$ $\mu A/cm^2$). Three other circumstances have recently been described in cardiac oscillators in which the transition is not direct. In all three cases, type 1 phase resetting is seen at low amplitudes, type 0 is seen at high amplitudes, and phase resetting to which a topological type or degree cannot be assigned is seen over an intermediate range of stimulus amplitudes.

In the first case, it is possible to annihilate spontaneous activity with a pulse of intermediate amplitude, because of the presence of at least one equilibrium point that is stable. This can be seen in the SAN (24), depolarized Purkinje fiber (25, 44), depolarized ventricular muscle (12, 44), and ionic models thereof (unpublished data; Refs. 7 and 8, respectively). Note that annihilation cannot occur in the model we have studied, because there is only one equilibrium point present (Fig 6*B* of Ref. 23), which numerical simulation reveals to be unstable.

In the second case, because of the presence of a saddle equilibrium point in the system, the topological degree of the phase resetting is also indeterminate over an intermediate range of stimulus amplitudes (10, 14). In this case, the saddle point arises via a saddle-node bifurcation; such a bifurcation hinges on there being a region of negative slope in the steady-state *I-V* curve (10). Whereas the SAN model studied here possesses an N-shaped *I-V* curve, many specimens of the SAN apparently do not possess such an N-shaped *I-V* curve (e.g., Ref. 40). In addition, because the negative resistance region of the N-shaped curve, when present, tends to be quite shallow in the SAN [unlike for example, in Purkinje fiber or ventricular cells (40)], it would be difficult, indeed perhaps even impossible, to clearly distinguish experimentally this indeterminate case of phase resetting from type 1 and type 0 phase resetting. This is true even in modeling work; in fact, in one recent study of a model containing a saddle point in which type 0 phase-resetting was said to exist (Fig. 8*C* of Ref. 43), it is not clear that a sufficiently high pulse amplitude was used to indeed obtain type 0 phase resetting. In addition, Φ'_1 was used to approximate Φ'_∞, which will lead to errors of interpretation as outlined above.

In the third case, seen in Purkinje fiber (28) and in embryonic chick ventricular heart cell aggregates (19), there is an intermediate range of stimulus amplitude over which the membrane demonstrates all-or-none depolarization. Modeling work in both these cases suggests that this behavior hinges upon the presence of I_{Na} (15, 18). One would therefore not expect to see such behavior in cells taken from the central region of the SAN, which possesses little I_{Na}. However, one would expect that it might be seen in spontaneously active cells taken from more peripheral regions of the SAN, where I_{Na} appears to be present in significantly larger amounts. Note that even in the model considered above, which does not contain much I_{Na}, the transition from maximal prolongation to maximal shortening of the cycle length T_1 can be very abrupt, taking place with a change in t_c of a few milliseconds at a stimulus amplitude just below that at which the type 1/type 0 border is attained (Fig. 4*C*).

Another circumstance in which a topological degree cannot be ascribed to the phase-resetting response, caused by all-or-none behavior, has recently been described in experiments on the SAN involving vagal stimulation (Fig. 2 of Ref. 30). It is possible that type 0 resetting would also have been seen in that case if the magnitude of vagal stimulation would have been further increased. However, the discontinuity seen in this instance might be caused by the fact that propagation of the cardiac impulse is all-or-none, and the phase-resetting response was measured at a site in the right atrium, not the sinoatrial node.

As stimulus amplitude is increased in the model, there is a direct transition from type 1 to type 0 phase resetting at $A \simeq -1.8$ $\mu A/cm^2$. Before this transition occurs, there is a change in the structure of the type 1 curve; it becomes nonmonotonic at $A \simeq -1.3$ $\mu A/cm^2$, and then has two extrema, one a minimum and the other a maximum. A similar change is seen in response to hyperpolarizing input. Note that this change is obligatory because, as stimulus amplitude increases, there is no way of continuously distorting a monotonic curve of degree one into a curve of degree zero. The existence of this nonmonotonicity has not previously been pointed out in modeling or experimental work on the SAN. Note that the type 0 curve is also, by definition, nonmonotonic, and that at $A = -2.0$ $\mu A/cm^2$ (Fig. 6, *C* and *D*) it also possesses two extrema. Nonmonotonicity (also termed noninvertibility) of the PTC has important consequences when a limit-cycle oscillator is periodically stimulated; for example, the existence of one extremum can result in period-doubling bifurcations, leading to alternans pat-

terns (13, 15–17, 21); a cascade of such bifurcations can lead to "chaotic" dynamics (13, 15–17, 21); and the existence of two extrema can produce bistability, the coexistence of two different synchronization patterns, leading to hysteresis (13, 15, 16, 21). Because there are amplitudes at which PTC_∞ possesses four extrema (not shown), the possibility of quadristability is also raised. Such four-extrema PTCs have recently been described in ionic models of Purkinje fiber (18) and depolarized ventricular muscle (29). It remains to be seen whether the above phenomena, predicted to exist from the phase-resetting response, are indeed present in the model when it is subjected to periodic stimulation.

Induction of a rotor. Repetitive activity at a fast rate can sometimes be seen in the SAN when a premature stimulus of the correct timing is delivered to the atrium (4, 33). It is generally accepted that these nondriven repetitive extrasystoles are caused by reentrant activity produced when the stimulus falls sufficiently early in the cycle so as to encounter refractoriness and produce block somewhere in the SAN itself or in the surrounding perinodal tissue. A theoretical mechanism for producing, de novo, a focus of activity ("rotor") in a spatially distributed, spontaneously oscillating medium by injecting a stimulus of the proper amplitude and timing has recently been propounded by Winfree (50). This mechanism hinges on the ability to obtain type 0 phase resetting. We have identified the waveforms in Fig. 3*C* as corresponding to type 0 phase resetting. Because, as previously mentioned, similar waveforms can be seen in the node in response to premature atrial stimulation, we can therefore conclude that the propagated atrial impulse is sufficiently strong to produce type 0 phase resetting of nodal cells. Thus the amplitude requirement (50) for provoking a rotor is satisfied. The traces shown in Fig. 7 indicate that the stable manifold of the only equilibrium point in the model studied above is encountered at a coupling interval such that the stimulus falls during the latter part of the repolarization phase of the action potential. The critical timing of the premature stimulus theoretically needed to induce a rotor coincides with this time (Ref. 50; see also Fig. 2-26 and associated explanation in Ref. 15); moreover, this time coincides with the "vulnerable period" during which rapid repetitive activity can indeed be induced experimentally. Thus both the amplitude and timing criteria for induction of a rotor in a spontaneously active medium are satisfied. Winfree's theory for the initiation and maintenance of a rotor can also be extended to the case of a quiescent, but excitable, medium (50); there is recent experimental evidence in quiescent ventricular muscle that lends support to this extension of the theory (9).

In conclusion, with one major exception reported on above, the absence of significant depression of automaticity, the model of Irisawa and Noma (23) replicates to a large extent the voltage waveforms seen during phase-resetting experiments. This exception might not be caused by any intrinsic shortcoming in the description of a patch of isopotential SAN membrane provided by the model but rather may be caused by propagation and electrotonic effects (46) that are necessarily excluded in our simulations. Indeed, some phenomena that can be seen in response to premature stimulation, such as pacemaker shift (4), will, by definition, only exist if there is a distributed pacemaker complex. Nevertheless, we find it rather surprising that a relatively simple model, encompassing only six currents, performs so well. Because I_{Na} and I_h do not play a great role in the Irisawa-Noma model, removal of these two currents results in almost unchanged behavior (the sole exception being that the increases in overshoot potential and upstroke potential beyond the normal value by a pulse delivered late in the cycle are then absent). Thus a four-variable model (*V, d, f,* and *p*) containing only the three currents I_s, I_K, and I_l would suffice to account, by and large, for the phase-resetting characteristics of the SAN

APPENDIX

A brief introduction to phase resetting, stressing topological concepts, is given by the following. More detailed information about the concepts outlined below can be found in the textbooks of Pavlidis (41) and Winfree (49, 50), as well as in two review articles (14, 31).

Phase shift, old phase, and new phase. When a brief-duration stimulus is applied to an oscillator, there is generally a transient speeding up or slowing down of the oscillator. Although the oscillator's period will eventually come back to its preexisting control value, the oscillator will in general suffer a permanent resetting of its rhythm. Figure 10 illustrates this concept, using a computer simulation of the ionic model of the sinoatrial node (23) studied in the body of this paper. Figure 10*A* shows an unperturbed control, whereas Fig. 10*B* shows the effect of injecting a stimulus that is a brief pulse of current. In this case, the stimulus causes a transient slowing of beat rate but a permanent shifting or resetting of the rhythm of the oscillator. For example, action potential upstrokes, which occur simultaneously in the two traces of Fig. 10 before injection of the stimulus pulse, are no longer synchronous after stimulus injection, even after waiting for a very long time. In experimental work, if one waits for a time long enough for the cycle to regain its original control period, one notices that there is a permanent temporal shift ΔT_∞ established between the timing of the upstroke of the control oscillator and that of the phase-shifted oscillator (Fig. 10). Note that ΔT_∞ is mathematically defined as the difference in the times at which the *i*th upstrokes occur in the two traces of Fig. 10 in the limit $i \rightarrow \infty$, hence the subscript ∞. Also by definition, the sign of ΔT_∞ is arbitrarily taken as being negative for the example shown in Fig. 10*B*, because the upstroke of the *i*th action potential in the perturbed trace occurs after that in the control trace in the limit $i \rightarrow \infty$.

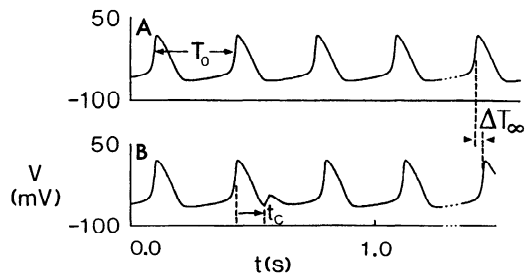

FIG. 10. *A*: unperturbed control activity in Irisawa-Noma (23) model. *B*: phase resetting produced by injecting a stimulus, a depolarizing current pulse of duration 20 ms and amplitude -1.5 $\mu A/cm^2$, at a coupling interval of $t_c = 120$ ms.

The phase shift $\Delta\Phi_\infty$ is defined as

$$\Delta\Phi_\infty = \begin{cases} \Delta T_\infty/T_0 \text{ (modulo 1)}, & \text{for } -0.5 \le \Delta T_\infty/T_0 \text{ (modulo 1)} < 0.5 \\ \Delta T_\infty/T_0 \text{ (modulo 1)} + 1, & \text{for } \Delta T_\infty/T_0 \text{ (modulo 1)} < -0.5 \\ \Delta T_\infty/T_0 \text{ (modulo 1)} - 1, & \text{for } \Delta T_\infty/T_0 \text{ (modulo 1)} \ge 0.5 \end{cases} \quad (A1)$$

Thus when $\Delta T_\infty = 0$, $\Delta\Phi_\infty = 0$, and there is no phase shift. For $\Delta\Phi_\infty < 0$, one speaks of a "phase delay," whereas for $\Delta\Phi_\infty \ge 0$, one has a "phase advance." Because a phase advance of one-half cycle is equivalent to a phase delay of one-half cycle, one must restrict $\Delta\Phi_\infty$ to the range $-0.5 \le \Delta\Phi_\infty < 0.5$. Given that it is possible in general for ΔT_∞ to exceed T_0 in magnitude, e.g., when a very long prolongation in cycle length is produced (e.g., Fig. 5 of Ref. 19), the fractional part of $\Delta T_\infty/T_0$ must be taken as indicated by the (modulo 1) operation in *Eq. A1*. We define the modulo 1 operation to be such that x (modulo 1), for x, a real number (positive or negative), is given by $x - [x]$, where $[x]$ indicates the integer (positive or negative) produced by truncating x, i.e., by removing its fractional part. Because $\Delta T_\infty/T_0$(modulo 1) thus gives values lying between -1 and $+1$, values equal to or bigger than 0.5 or more negative than -0.5 must then be converted to values lying in the range $-0.5 \le \Delta\Phi_\infty < 0.5$ by subtracting 1 or adding 1, respectively, as in *Eq. A1*.

One can also define the phase shift as the difference between the new phase and the old phase. To do so, one must first define these two phases. The phase in the cycle at which the stimulus is injected is given simply by t_c/T_0, where T_0 is the intrinsic cycle length of the oscillator, and t_c is the coupling interval at which the pulse is injected (Fig. 10). This particular phase is called the old phase and is denoted by Φ

$$\Phi = t_c/T_0 \quad (A2)$$

It is termed the old phase, because it indicates the phase of the oscillator just before delivery of the phase-shifting stimulus. As a result of its definition as the fractional part of the cycle at which the stimulus is injected, one has $0 \le \Phi < 1$. For example, a stimulus pulse injected at the beginning of the cycle is delivered at $\Phi = 0.0$, whereas one injected halfway through the cycle is delivered at $\Phi = 0.5$.

The new phase or "eventual phase" Φ'_∞ depends on the magnitude and sign of the phase shift $\Delta\Phi_\infty$ produced by the stimulus, and is defined by

$$\Phi'_\infty = (\Phi + \Delta T_\infty/T_0) \text{ (modulo 1)} + N \quad (A3)$$

where N is the smallest positive integer ensuring $\Phi'_\infty \ge 0$. The subscript ∞ indicates that the new phase is measured an infinitely long time after delivery of the stimulus. Thus at values of Φ where $\Delta T_\infty = 0$, Φ'_∞ will equal Φ (the new phase will equal the old phase), and no phase shift will have occurred. Because the old phase has the range $0 \le \Phi < 1$, one allows the same range for the new phase, i.e., $0 \le \Phi'_\infty < 1$, so as to be able to compare new phase with old phase. The fractional part of the term $\Phi + \Delta T_\infty/T_0$ appearing in the right-hand side of *Eq. A3* must be taken [using the modulo 1 operation], because it is possible for this sum to equal or exceed unity if ΔT_∞ is sufficiently large. For example, a stimulus that causes a prolongation of exactly two cycle lengths does not produce any phase shift by this definition, because $\Phi'_\infty = \Phi$. Also, because $(\Phi + \Delta T_\infty/T_0)$(modulo 1) can be negative (e.g., if ΔT_∞ is sufficiently negative and Φ sufficiently small), one must convert such a negative value to a positive value by adding the smallest positive integer (N) that ensures that Φ'_∞ is nonnegative. Finally, the definition of phase shift $\Delta\Phi_\infty$, which must have the range $-0.5 \le \Delta\Phi_\infty < 0.5$, can now be given in terms of new phase and old phase

$$\Delta\Phi_\infty = \begin{cases} \Phi'_\infty - \Phi, & \text{for } -0.5 \le \Phi'_\infty - \Phi < 0.5 \\ \Phi'_\infty - \Phi + 1, & \text{for } \Phi'_\infty - \Phi < -0.5 \\ \Phi'_\infty - \Phi - 1, & \text{for } \Phi'_\infty - \Phi \ge 0.5 \end{cases} \quad (A4)$$

Note that ΔT_∞, $\Delta\Phi_\infty$, and Φ'_∞ depend both on stimulus timing (i.e., t_c or Φ) and the stimulus parameters, i.e., stimulus polarity, amplitude, and duration. For a given combination of stimulus parameters, one can investigate in a systematic manner the effect of changing the old phase Φ. One can then measure ΔT_∞, calculate the phase shift $\Delta\Phi_\infty$ from *Eq. A1*, and plot the phase shift $\Delta\Phi_\infty$ vs. the old phase Φ. This curve is called the phase response curve (PRC). At a small stimulus strength, a plot such as that shown in Fig. 11*A* results in many biological preparations (49). There is a range of Φ over which $\Delta\Phi_\infty < 0$ (i.e., the oscillator is phase delayed), whereas over another range $\Delta\Phi_\infty > 0$ (i.e., the oscillator is phase advanced). One can also calculate Φ'_∞ from *Eq. A3*, and plot the new phase Φ'_∞ vs. the old phase Φ. This curve is called the new phase-old phase curve or the phase transition curve (PTC). Figure 11*B* shows the PTC corresponding to the PRC of Fig. 11*A*. Note that in the limit of zero-stimulus strength, $\Delta\Phi_\infty = 0$, independent of Φ, and so the PRC approaches the horizontal straight line $\Delta\Phi_\infty = 0$ in that limit, whereas the PTC approaches the diagonal line $\Phi'_\infty = \Phi$.

The phase shift $\Delta\Phi_\infty$ in Fig. 11*A* does not span the full range $-0.5 \le \Delta\Phi_\infty < 0.5$. It is only at a sufficiently high stimulus amplitude that all possible values of $\Delta\Phi_\infty$ will be encountered. Figure 11, *C* and *D*, shows the PRC and PTC, respectively, in this case. These two curves are not discontinuous, because a phase shift of 0.5 is equivalent to a phase shift of -0.5, and a new phase of 1.0 is equivalent to a new phase of 0.0. Note that the old phase Φ where $\Delta\Phi_\infty = 0.5$ is not the same as that at which $\Phi'_\infty = 0$.

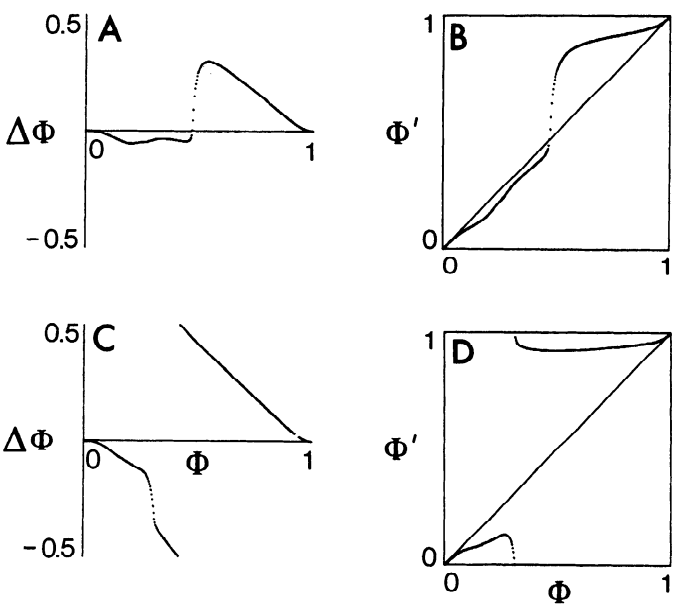

FIG. 11. Phase response curves (*A*, *C*) and phase transition curves (*B*, *D*) at low (top row: amplitude = -1.0 $\mu A/cm^2$) and high (bottom row: amplitude = -2.0 $\mu A/cm^2$) levels of stimulus amplitude, corresponding to type 1 and type 0 phase resetting, respectively. Second transient phase (*B*, *D*) and phase shift (*A*, *C*) are shown in these curves (see text).

There is a qualitative difference in the two curves of Fig. 11, *B* and *D*, the first being obtained at a sufficiently low stimulus strength and the second at a sufficiently high strength. The average slope of the PTC in Fig. 11*B* is 1, the curve is of topological degree 1, and thus type 1 phase resetting is said to occur (49). In contrast, in Fig. 11*D*, the average slope is zero, the curve is of topological degree 0, and so type 0 phase resetting occurs (49).

Isochrons. These two qualitatively different kinds of PTC have been seen in phase-resetting experiments carried out on many biological oscillators (49). Why are these two types, and no others, seen? The answer to this question, as initially pointed out by Winfree (49), lies in the qualitative theory of differential equations. The oscillation in Fig. 10*A* is described by a set of differential equations; indeed, it is this set of equations, forming a model for the sinoatrial node, that we numerically integrate to produce the trace shown in Fig. 10*A*. In this model, at any time t, the state of the system is completely specified by the values of the seven variables of the system at that time. These variables are the transmembrane potential V, and the six activation and inactivation variables (m, h, d, f, p, and q) that gate the various ionic currents in the model. The state space of the system is thus seven-dimensional, with the state of the system at any point in time being specified by the position of a point, the state point, in that seven-dimensional space. As the system evolves in time, the state point traces out a curve in the state space called a trajectory. Thus the usual cyclic activity seen in the model and responsible for producing the voltage trace shown in Fig. 10*A* corresponds to movement of the state point along a closed trajectory called a limit cycle.

Because it is difficult to visualize events occurring in a seven-dimensional space, we use the simple two-dimensional limit-cycle oscillator shown in Fig. 12*A* to illustrate Winfree's theory. The thick closed curve with the arrow is the limit cycle itself. As time proceeds, the state point of the system moves along this cycle in the direction of the arrow, generating a repetitive cyclic waveform for both variables (x and y) of the system. Let us now perform a phase-resetting experiment by injecting a stimulus when the state point is at the point labeled *a* on the cycle (Fig. 12*A*), corresponding to an old phase of, say, 0.0. During the time that the stimulus is on, the state point will move away from its usual path along the limit cycle and will instead move along the trajectory from *point a* to *point b*. When the stimulus is turned off at *point b*, the trajectory will then relax back toward the limit cycle along the path illustrated. Mathematically, even though this trajectory approaches the limit cycle more closely as time goes on, it never really returns to it in finite time. Let us assume that the corresponding new phase (Φ'_∞) in this example is 0.1. By continuity, there will be a set of points close to *b* with the property that if at the end of a stimulus pulse, the state point coincides with any one of these points, the new phase will also be 0.1. This set of points forms a curve that will thread through the limit cycle. Note that this curve, called an isochron, must intersect the limit cycle at a point, *c*, where the old phase is 0.1 (Fig. 12*B*), because, should a stimulus deliver the state point to *point c*, one would have a new phase of 0.1. There are infinitely many isochrons, one for each value of Φ'_∞, threading through the limit cycle. In Fig. 12*B*, we show the 0.1, 0.3, 0.5, 0.7, and 0.9 isochrons. In Fig. 12*C*, injection of a stimulus at an old phase of, say, 0.6, causes the state point to move from *d* to *e*, which lies on the 0.5 isochron. By starting out from many old phases on the limit cycle, the dashed curve in Fig. 12*C* can be constructed. This curve is the shifted cycle, which defines the locus of the state point at the end of the stimulus pulse for any old phase, i.e., it is the locus of all points such as *b* and *e* shown as specific examples in Fig. 12*C*. Note that in the case of Fig. 12*C*, the shifted cycle intersects all isochrons between 0.0 and 1.0; thus given any

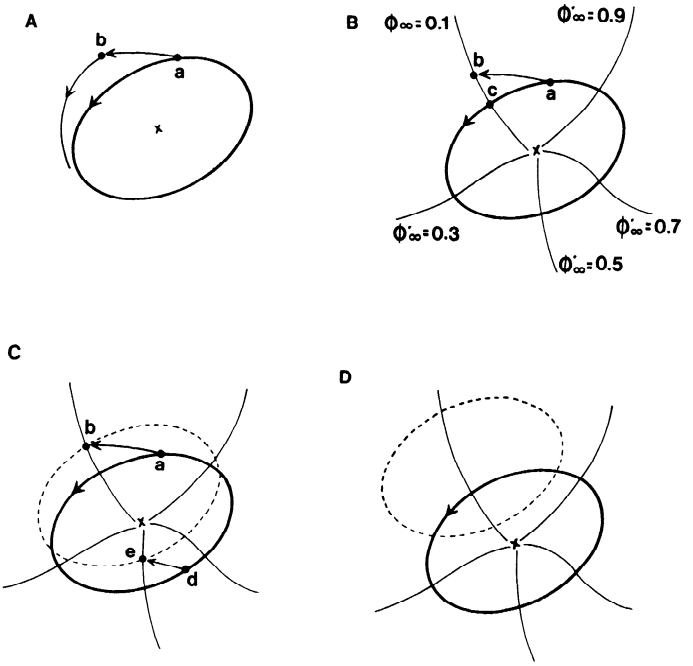

FIG. 12. Simple 2-dimensional limit-cycle oscillator (*A*) used to illustrate concept of isochron (*B*) and genesis of type 1 (*C*) and type 0 (*D*) phase resetting. See text for further explanation.

arbitrary isochron with a particular new phase, there is always some old phase, starting from which that new phase is accessible. This results in a type 1 new phase-old phase curve, similar to that shown in Fig. 11*B*.

As stimulus amplitude is increased, the effect of the perturbation will be greater, and the shifted cycle will move further away from the limit cycle. Eventually, a situation such as that shown in Fig. 12*D* will result. Note that the shifted cycle no longer intersects all of the isochrons. In fact, isochrons with new phase in the range from ~0.3 to 0.9 are not accessible in this particular case, no matter at what old phase the stimulus pulse is injected. Thus a gap will appear in the new phase values of the new phase-old phase curve, as in the type 0 curve of Fig. 11*D*. Note also that each of the accessible isochrons (e.g., $\Phi'_\infty = 0.1$ in Fig. 12*D*) has two intersections with the shifted cycle, meaning that any accessible new phase can be reached from two different values of the old phase (see also Fig. 11*D*).

At one definite stimulus amplitude somewhere between those used in Fig. 12, *C* and *D*, one point on the shifted cycle will coincide with the equilibrium point in the interior of the limit cycle (indicated by the symbol x). Because this is an equilibrium point, the state point will rest there indefinitely (in a noise-free system) after stimulation, oscillation will cease, and the new phase will be undefined for the corresponding old phase. It is precisely at this amplitude that the type 1/type 0 border is encountered. In a state space of dimension greater than 2, this border occurs at the amplitude where the shifted cycle encounters the stable manifold of the equilibrium point, which is not a point but a higher-dimensional object such as a curve (49). (Also in that case, the isochrons are not one-dimensional curves; for example, in the seven-dimensional ionic model studied here, the isochrons are six-dimensional hypersurfaces.) The traces of Fig. 7 are similar to what one would expect when the state point of the system lies very close to the stable manifold after stimulus injection, because they show incrementing low-amplitude oscillatory activity; indeed the traces are quite similar to what one sees if one starts the simulation with initial conditions close to the equilibrium point in the

model. This interpretation is also consistent with the fact that the stimulus amplitude at which these traces are found lies just above that defining the type 1/type 0 border.

Discontinuities in phase resetting. So far, we have characterized the phase-resetting response in the limit of waiting for an infinitely long time (Fig. 10), because it is only in that limit that the trajectory theoretically returns to the limit cycle after a perturbation (Fig. 12*A*). However, in experimental and modeling work, one must perforce acquire data at a finite time after delivery of the stimulus. In addition, real systems are "noisy," and one can imagine that it would suffice in Fig. 12*A* that the corresponding noisy trajectory originating at *point b* simply enters the region of phase space wherein the noisy limit cycle is circulating. As a rule of thumb, one can reliably estimate the new phase once the cycle length has returned to within a few percent of its control value. In cardiac phase-resetting studies involving current-pulse injection, this usually occurs within a few cycles (15).

However, if one does not wait for a sufficiently long time, which has been a common practice in previous experimental and modeling work, the characteristics of the phase-resetting response can be quite altered. The most extreme example of this is perhaps seen if one considers the timing of the upstroke immediately after delivery of the stimulus. In that case, one can define the first transient new phase Φ_1' in a manner analogous to that in which Φ_∞' was earlier defined in *Eq. A3*

$$\Phi_1' = (\Phi + \Delta T_1/T_0) \text{ (modulo 1)} + N \qquad (A5)$$

where T_1 is as indicated in Fig. 2. Note that defining an absolute time T_1 requires a precise, but arbitrary, definition of when the upstroke occurs. In the body of this paper, we have chosen a positive-going crossing of −10 mV of the transmembrane potential V as our definition of this event marker. In the seven-dimensional phase space of the ionic model, an event thus occurs when the trajectory pierces the hyperplane $V = -10$ mV in the direction corresponding to increasing V. One can in general define the ith transient new phase Φ_i'

$$\Phi_i' = (\Phi + \Delta T_i/T_0) \text{ (modulo 1)} + N \qquad (A6)$$

where the ΔT_is are as indicated in Fig. 2. A plot of Φ_i' vs. Φ is called the ith transient phase transition curve (PTC_i). Discontinuous jumps will exist in general (31) in all of the PTC_i (e.g., see Φ_1' in middle and bottom rows of Fig. 6). However, the size of these jumps will decrease as i increases. In fact, in the limit $i \to \infty$, it can be proven mathematically that these Kawato-Suzuki "discontinuities of the first kind" must heal up, resulting in a PTC_∞ that is continuous (31). Again, the rate at which the discontinuity heals up will depend on how quickly the trajectory returns to the limit cycle after a perturbation. On the scale of the computations shown in this paper, no discontinuities are visible in PTC_2 (see Φ_2' curves in Fig. 6); indeed, PTC_2 is superimposable with PTC_3, and so PTC_2 can be taken as a very good approximation to PTC_∞. In fact, in Fig. 11 we actually show Φ_2' and the second transient phase shift $\Delta\Phi_2$ (which is defined as in *Eq. A1*, replacing $\Delta\Phi_\infty$ with $\Delta\Phi_2$ and ΔT_∞ with ΔT_2). In situations in which the effect of the perturbation on the oscillator is longer lasting (e.g., vagal stimulation of the sinoatrial node), one might have to examine PTC_i for $i \geq 4$. The origin of the discontinuities in PTC_i can be understood if one considers how the shifted cycle of Fig. 12, *C* and *D*, intersects the event marker surface; for a graphical illustration of this fact in a simple two-variable model, see Fig. 5 of Ref. 31 and associated explanation.

We thank Antoni van Ginneken for helpful conversations and comments on the manuscript. We also thank Christine Pamplin, Diane Colizza, and Sandra James for typing the manuscript, A. van Horssen for drafting Fig. 12, and Martijn Overzier and Robert Thomson for photographing the figures.

M. R. Guevara thanks the Canadian Heart Foundation and the Natural Sciences and Engineering Research Council of Canada for postdoctoral fellowship support (1984–86). The study was supported by grants to H. J. Jongsma from the Dutch Organization for Pure Research and to M. R. Guevara from the Medical Research Council of Canada.

Address for reprint requests: M. R. Guevara, Dept. of Physiol., McGill Univ., 3655 Drummond Street, Montreal, Quebec H3G 1Y6, Canada.

Present address of H. J. Jongsma: Fysiologisch Laboratorium, Universiteit van Amsterdam, Subfaculteit der Geneeskunde, Academisch Medisch Centrum, Meibergdreef 15, 1105 AZ Amsterdam, The Netherlands.

Received 19 November 1987; accepted in final form 20 October 1989.

REFERENCES

1. BELLET, S. *Clinical Disorders of the Heart Beat* (3rd ed.). Philadelphia, PA: Lea & Febiger, 1971, p. 386.
2. BEST, E. N. Null space in the Hodgkin-Huxley equations: a critical test. *Biophys. J.* 27: 87–104, 1979.
3. BLEEKER, W. K., A. J. C. MACKAAY, M. MASSON-PÉVET, L. N. BOUMAN, AND A. E. BECKER. Functional and morphological organization of the rabbit sinus node. *Circ. Res.* 46: 11–22, 1980.
4. BONKE, F. I. M., L. N. BOUMAN, AND F. J. G. SCHOPMAN. Effect of an early atrial premature beat on activity of the sinotrial node and atrial rhythm in the rabbit. *Circ. Res.* 29: 704–715, 1971.
5. BRISTOW, D. G., AND J. W. CLARK. A mathematical model of primary pacemaking cell in SA node of the heart. *Am. J. Physiol.* 243 (*Heart Circ. Physiol.* 12): H207–H218, 1982.
6. BROWN, H., J. KIMURA, AND S. NOBLE. The relative contributions of various time-dependent membrane currents to pacemaker activity in the sino atrial node. In: *Cardiac Rate and Rhythm*, edited by L. N. Bouman and H. J. Jongsma. The Hague: Nijhoff, 1982, p. 53–68.
7. CHAY, T. R., AND Y. S. LEE. Impulse responses of automaticity in the Purkinje fiber. *Biophys. J.* 45: 841–869, 1984.
8. CHAY, T. R., AND Y. S. LEE. Phase resetting and bifurcation in the ventricular myocardium. *Biophys. J.* 47: 641–651, 1985.
9. CHEN, P.-S., P. D. WOLF, E. G. DIXON, N. D. DANIELEY, D. W. FRAZIER, W. M. SMITH, AND R. E. IDEKER. Mechanism of ventricular vulnerability to single premature stimuli in open-chest dogs. *Circ. Res.* 62: 1191–1209, 1988.
10. CLAY, J. R., M. R. GUEVARA, AND A. SHRIER. Phase resetting of the rhythmic activity of embryonic heart cell aggregates: experiment and theory. *Biophys. J.* 45: 699–714, 1984.
11. DÓRTICOS, F. R., J. O. BUSTAMANTE, J. ÁLVAREZ, AND J. MORLANS. Effects of atrial premature stimulation on sinus node function in isolated rabbit atria. *Cor Vasa* 20: 417–428, 1978.
12. GILMOUR, R. F., JR., J. J. HEGER, E. N. PRYSTOWSKY, AND D. P. ZIPES. Cellular electrophysiologic abnormalities of diseased human ventricular myocardium. *Am. J. Cardiol.* 51: 137–144, 1983.
13. GLASS, L., M. R. GUEVARA, J. BELAIR, AND A. SHRIER. Global bifurcations of a periodically forced biological oscillator. *Phys. Rev. A* 29: 1348–1357, 1984.
14. GLASS, L., AND A. T. WINFREE. Discontinuities in phase-resetting experiments. *Am. J. Physiol.* 246 (*Regulatory Integrative Comp. Physiol.* 15): R251–R258, 1984.
15. GUEVARA, M. R. *Chaotic Cardiac Dynamics* (PhD thesis). Montreal, Canada: McGill Univ., 1984.
16. GUEVARA, M. R., L. GLASS, M. C. MACKEY, AND A. SHRIER. Chaos in neurobiology. *IEEE Trans. Syst. Man Cybern.* SMC-13: 790–798, 1983.
17. GUEVARA, M. R., L. GLASS, AND A. SHRIER. Phase locking, period-doubling bifurcations, and irregular dynamics in periodically stimulated cardiac cells. *Science Wash. DC* 214: 1350–1353, 1981.
18. GUEVARA, M. R., AND A. SHRIER. Phase resetting in a model of cardiac Purkinje fibre. *Biophys. J.* 52: 165–175, 1987.
19. GUEVARA, M. R., A. SHRIER, AND L. GLASS. Phase resetting of spontaneously beating embryonic ventricular heart cell aggregates. *Am. J. Physiol.* 251 (*Heart Circ. Physiol.* 20): H1298–H1305, 1986.
20. GUEVARA, M. R., A. SHRIER, AND L. GLASS. Phase-locked rhythms

in periodically stimulated heart cell aggregates. *Am. J. Physiol.* 254 (*Heart Circ. Physiol.* 23): H1–H10, 1988.
21. GUEVARA, M. R., A. SHRIER, AND L. GLASS. Chaotic and complex cardiac rhythms. In: *Cardiac Electrophysiology: From Cell to Bedside*, edited by D. P. Zipes and J. Jalife. Philadelphia, PA: Saunders. In press.
22. HERBERT, W. H. The effect of ventricular action currents on the sinoatrial node. *J. Electrocardiol. San Diego* 3: 121–126, 1970.
23. IRISAWA, H., AND A. NOMA. Pacemaker mechanisms of rabbit sinoatrial node cells. In: *Cardiac Rate and Rhythm*, edited by L. N. Bouman and H. J. Jongsma. The Hague: Nijhoff, 1982, p. 35–51.
24. JALIFE, J., AND C. ANTZELEVITCH. Phase resetting and annihilation of pacemaker activity in cardiac tissue. *Science Wash. DC* 206: 695–697, 1979.
25. JALIFE, J., AND C. ANTZELEVITCH. Pacemaker annihilation: diagnostic and therapeutic implications. *Am. Heart J.* 100: 128–129, 1980.
26. JALIFE, J., A. J. HAMILTON, V. R. LAMANNA, AND G. K. MOE. Effects of current flow on pacemaker activity of the isolated kitten sinoatrial node. *Am. J. Physiol.* 238 (*Heart Circ. Physiol.* 7): H307–H316, 1980.
27. JALIFE, J., AND D. C. MICHAELS. Phase-dependent interactions of cardiac pacemakers as mechanisms of control and synchronization in the heart. In: *Cardiac Electrophysiology and Arrhythmia*, edited by D. P. Zipes and J. Jalife. Orlando, FL: Grune & Stratton, 1985, p. 109–119.
28. JALIFE, J., AND G. K. MOE. Effect of electrotonic potentials on pacemaker activity of canine Purkinje fibers in relation to parasystole. *Circ. Res.* 39: 801–808, 1976.
29. KAPRAL, R. Stochastic dynamics of limit-cycle oscillators with vulnerable phases. *J. Chim. Phys.* 84: 1295–1303, 1985.
30. KAREMAKER, J. M. Relations between changes in cardiac parasympathetic activity and heart rate variability. In: *Cardiorespiratory and Cardiosomatic Psychophysiology*, edited by P. Grossman, K. H. L. Janssen, and D. Vaitl. New York: Plenum, 1986, p. 55–61.
31. KAWATO, M. Transient and steady state phase response curves of limit cycle oscillators. *J. Math. Biol.* 12: 13–30, 1981.
32. KERR, C. R., E. N. PRYSTOWSKY, D. J. BROWNING, AND H. C. STRAUSS. Characterization of refractoriness in the sinus node of the rabbit. *Circ. Res.* 47: 742–756, 1980.
33. KLEIN, H. O., D. H. SINGER, AND B. F. HOFFMAN. Effects of atrial premature systoles on sinus rhythm in the rabbit. *Circ. Res.* 32: 480–491, 1973.
34. KODAMA, I., AND M. R. BOYETT. Regional differences in electrical activity of the rabbit sinus node. *Pfluegers Arch.* 404: 214–226, 1985.
35. KREITNER, D. Electrophysiological study of the two main pacemaker mechanisms in the rabbit sinus node. *Cardiovasc. Res.* 19: 304–318, 1985.
36. MICHAELS, D. C., E. P. MATYAS, AND J. JALIFE. Dynamic interaction and mutual synchronization of sinoatrial node pacemaker cells. A mathematical model. *Circ. Res.* 58: 706–720, 1986.
37. NILIUS, B. Possible functional significance of a novel type of cardiac Ca channel. *Biomed. Biochim. Acta* 45: K37–K45, 1986.
38. NOBLE, D., AND S. J. NOBLE. A model of sino-atrial node electrical activity based on a modification of the DiFrancesco-Noble equations. *Proc. R. Soc. Lond. B Biol. Sci.* 222: 295–304, 1984.
39. NOMA, A., AND H. IRISAWA. Effects of Na^+ and K^+ on the resting membrane potential of the rabbit sinoatrial node cell. *Jpn. J. Physiol.* 25: 287–302, 1975.
40. NOMA, A., T. NAKAYAMA, Y. KURACHI, AND H. IRISAWA. Resting K conductances in pacemaker and non-pacemaker heart cells of the rabbit. *Jpn. J. Physiol.* 34: 245–254, 1984.
41. PAVLIDIS, T. *Biological Oscillators: Their Mathematical Analysis.* New York: Academic, 1973.
42. PICK, A., R. LANGENDORF, AND L. N. KATZ. Depression of cardiac pacemakers by premature impulses. *Am. Heart J.* 41: 49–57, 1951.
43. REINER, V. S., AND C. ANTZELEVITCH. Phase resetting and annihilation in a mathematical model of sinus node. *Am. J. Physiol.* 249 (*Heart Circ. Physiol.* 18): H1143–H1153, 1985.
44. ROSENTHAL, J. E., AND G. R. FERRIER. Contribution of variable entrance and exit block in protected foci to arrhythmogenesis in isolated ventricular tissues. *Circulation* 67: 1–8, 1983.
45. SANO, T., T. SAWANOBORI, AND H. ADANIYA. Mechanism of rhythm determination among pacemaker cells of the mammalian sinus node. *Am. J. Physiol.* 235 (*Heart Circ. Physiol.* 4): H379–H384, 1978.
46. STEINBECK, G., M. A. ALLESSIE, F. I. M. BONKE, AND W. J. E. P. LAMMERS. Sinus node response to premature atrial stimulation in the rabbit studied with multiple microelectrode impalements. *Circ. Res.* 43: 695–704, 1978.
47. USHIYAMA, J., AND C. MCC. BROOKS. Intracellular stimulation and recording from single cardiac cells in the rabbit atrium. *J. Electrocardiol.* 7: 119–126, 1974.
48. VICTORRI, B., A. VINET, F. A. ROBERGE, AND J.-P. DROUHARD. Numerical integration in the reconstruction of cardiac action potentials using Hodgkin-Huxley-type models. *Comp. Biomed. Res.* 18: 10–23, 1985.
49. WINFREE, A. T. *The Geometry of Biological Time.* New York: Springer-Verlag, 1980.
50. WINFREE, A. T. *When Time Breaks Down: The Three-Dimensional Dynamics of Electrochemical Waves and Cardiac Arrhythmias.* Princeton, NJ: Princeton Univ. Press, 1987.
51. YANIGIHARA, K., A. NOMA, AND H. IRISAWA. Reconstruction of sino-atrial node pacemaker potential based on the voltage clamp experiments. *Jpn. J. Physiol.* 30: 841–857, 1980.